partially negated by the higher MR and higher ρ of the geometric MR sensor. Furthermore, physical MR information storage sensors such as spin-valve read heads may not provide sufficient sensitivity when scaled to sizes corresponding to the superparamagnetic limit for modern media of 100 Gb/inch^2, because of demagnetization and other magnetic effects (*22*). Composite nonmagnetic semiconductors with enhanced geometric MR > ~100% at the relevant field (*23*), H_{rel} = 0.05 T, are not thus limited and could still exhibit high MR even when scaled to mesoscopic sizes (*24*). Also, their response time can be approximated by the inverse of the plasmon frequency, yielding a value in the subpicosecond range (*25*). This is substantially faster than the 10^{-9} to 10^{-10} s switching times of metallic sensors that are limited by magnetization dynamics (*22*). It should also be easy to provide the ~ 0.2 T self (*19*) or external biasing necessary to obtain a linear response and higher MR close to $H = 0$.

In addition to SNR, semiconductor physical MR sensors are often judged by a figure of merit $(1/R)(dR/dH)$ that typically exhibits a RT maximum of ~2.5 T^{-1} around a biasing field of 0.25 T (*2*). If we use this figure of merit, our MR sensor with α = 13/16 reaches a corresponding maximum of 24 T^{-1} at 0.13 T, a factor of ~10 improvement, realized at a lower field. InSb enhanced geometric MR sensors should also be competitive with InSb Hall sensors (*3*) now produced in quantities >10^9/year for motors in consumer electronics.

Finally, one can readily anticipate sensors with still higher geometric MR values than reported in this proof-of-principle study. With higher mobility films and more vertical inhomogeneity side walls, we believe a further improvement of a factor of 2 to 3 of the MR to be in comfortable reach. In addition, the simple vdP geometry may not be optimal. Whatever the ultimate magnitude of achievable MR, it is clear that careful design of simple composite metal-semiconductor structures can result in sensors with substantially enhanced RT geometric MR.

References and Notes

1. J. A. Brug, T. C. Anthony, J. H. Nickel, *MRS Bull.* **21**, 23 (1996).
2. J. P. Heremans, *Mat. Res. Soc. Symp. Proc.* **475**, 63 (1997).
3. N. Kuze and I. Shibasaki, *III-V's Rev.* **10**, 28 (1997).
4. H. H. Wieder, *Hall Generators and Magnetoresistors* (Pion, London, 1971).
5. R. S. Popovic, *Hall Effect Devices* (Hilger, Bristol, UK, 1991).
6. P. M. Levy, *Solid State Phys.* **47**, 367 (1994).
7. C. N. R. Rao and B. Raveau, Eds., *Colossal Magnetoresistance, Charge Ordering and Related Properties of Manganese Oxides* (World Scientific, Singapore, 1998).
8. W. F. Egelhoff Jr. *et al.*, *J. Appl. Phys.* **78**, 273 (1995).
9. S. Jin, M. McCormack, T. H. Tiefel, R. Ramesh, *J. Appl. Phys.* **76**, 6929 (1994).
10. T. Thio *et al.*, *Phys. Rev. B* **57**, 12239 (1998).
11. W. Zawadzki, *Adv. Phys.* **23**, 435 (1974).
12. C. Herring, *J. Appl. Phys.* **31**, 1939 (1960).
13. A. Y. Shik, *Electronic Properties of Inhomogeneous Semiconductors* (Gordon and Breach, Amsterdam, 1995).
14. H. Weiss and M. Wilhelm, *Z. Phys.* **176**, 399 (1963).
15. S. D. Parker *et al.*, *Semicond. Sci. Technol.* **4**, 663 (1989).
16. C. M. Wolfe, G. E. Stillman, J. A. Rossi, *J. Electrochem. Soc. Solid-State Sci. Technol.* **119**, 250 (1972).
17. S. P. S. Parkin, *Bull. Am. Phys. Soc.* **44**, 1555 (1999).
18. T. Thio and S. A. Solin, *Appl. Phys. Lett.* **72**, 3497 (1998).
19. S. A. Solin *et al.*, *Appl. Phys. Lett.* **69**, 4105 (1996).
20. S. A. Solin, T. Thio, D. R. Hines, T. Zhou, unpublished data.
21. H. Neal Bertram, *Theory of Magnetic Recording* (Cambridge Univ. Press, Cambridge, 1994).
22. K. O'Grady, R. L. White, P. J. Grundy, *J. Magn. Magn. Mater.* **177–181**, 886 (1998).
23. The relevant field is the field that the sensor can access for a given read-head design with modern disk media.
24. For mesoscopic devices such as 100 Gb/inch^2 read-head sensors, we would use structures with lateral dimensions of order L ~ 100 nm and thickness of 30 nm. Such structures with α = 13/16 would have an effective resistance of order 1 to 2 ohm for $0 < H <$ 0.05 T. Because this resistance is $\ll h/e^2$, where h is Planck's constant, conductance fluctuations should not impact the geometric MR. However, μ_{app} scales with $\mu = e\tau/m^*$, where τ is the electron mean free scattering time and m^* is the effective mass. For sample dimensions $L > \lambda$, the mean free path, $\tau = \lambda/v_F$, where v_F is the Fermi velocity. But when $L < \lambda$, scattering at the boundary dominates and $\tau \sim L/v_F$, so μ_{app} will scale with L and the geometric MR will scale (down) with L^2. Fortunately, the same boundary scattering also gives rise to a geometric MR that increases with H (and is larger than that of bulk material) up to a field H_c above which the MR decreases with increasing H [see F. Rahman *et al.*, *Semicond. Sci. Technol.* **14**, 478 (1999)]. Here, H_c corresponds to a cyclotron diameter of order the device size. The fields of interest here for 100 Gb/inch^2 sensors are well below H_c. For the InSb studied here, λ ~ 300 nm so the above described mesoscopic effects will be important and worth investigating. We are now using state-of-the-art e-beam lithography to fabricate and study the properties of mesoscopic enhanced geometric MR sensors.
25. M. F. Hoyaux, *Solid State Plasmas* (Pion, London, 1970).

26. Part of the work by J.J.H. was performed at EMCORE, Somerset, NJ. We thank J. A. Giordmaine for stimulating our interest in this work and L. F. Cohen and B. Altshuler for several useful discussions. We also thank S. Schwed and M. W. Pelczynski (EMCORE) for assistance with sample preparation and processing.

1 June 2000; accepted 18 July 2000

Evidence for Superfluidity in Para-Hydrogen Clusters Inside Helium-4 Droplets at 0.15 Kelvin

Slava Grebenev,[1]* Boris Sartakov,[2] J. Peter Toennies,[1]† Andrei F. Vilesov[1]*

A linear carbonyl sulfide (OCS) molecule surrounded by 14 to 16 para-hydrogen (pH_2) molecules, or similar numbers of ortho-deuterium (oD_2) molecules, within large helium-4 (^{4}He) droplets and inside mixed ^{4}He/^{3}He droplets was investigated by infrared spectroscopy. In the pure ^{4}He droplets (0.38 kelvin), both systems exhibited spectral features that indicate the excitation of angular momentum around the OCS axis. In the colder ^{4}He/^{3}He droplets (0.15 kelvin), these features remained in the oD_2 cluster spectra but disappeared in the pH_2 spectra, indicating that the angular momentum is no longer excited. These results are consistent with the onset of superfluidity, thereby providing the first evidence for superfluidity in a liquid other than helium.

The helium liquids ^{4}He and ^{3}He are the only known substances that exhibit the phenomenon of superfluidity below transition temperatures T_c = 2.18 K and $T_c = 2.4 \times 10^{-3}$ K, respectively. Despite intensive theoretical and experimental efforts during the ~60 years since its discovery, this remarkable effect still eludes complete understanding (*1*). Thus, there is considerable interest in finding superfluidity in other substances, and this is one of the reasons for the great interest in the recently discovered phenomenon of Bose-Einstein condensation (BEC) in the alkali atom gases (*2*). In 1972, Ginzburg and Sobyanin (*3*) estimated the BEC temperature of the modification of hydrogen molecules with antiparallel spins on the two nuclei (i.e., para-H_2 or pH_2 molecules) to be T_c = 6 K. They used the formula

$$T_c = \frac{3.31\hbar^2}{g^{2/3} M k_B} n^{2/3} \quad (1)$$

[1]Max-Planck-Institut für Strömungsforschung, Bunsenstraße 10, 37073 Göttingen, Germany. [2]General Physics Institute, Russian Academy of Sciences, 117942 Moscow, Russia.

*Present address: Ruhr-University Bochum, Physical Chemistry II, D-44780 Bochum, Germany.
†To whom correspondence should be addressed. E-mail: jtoenni@gwdg.de

(*4*), where n is the particle density, g is the spin degeneracy of the particles (g = 1 for pH_2), M is their mass, $\hbar$ is Planck's constant divided by 2π, and k_B is the Boltzmann constant. According to Eq. 1, T_c is expected to be highest for pH_2 molecules in their rotational ground state (j = 0) because they have a nuclear spin of I = 0 and are therefore, like ^{4}He atoms, spinless bosons. In ortho-H_2 (I = 1, g = 3), T_c will be ~3 K, and in ortho-D_2 (1/6 in I = 0 and 5/6 in I = 2), superfluidity will be further impaired by the mixture of nuclear spin states, the greater degeneracy, and the greater mass. The triple point of hydrogen is 13.8 K, and the liquid therefore must be extensively supercooled to observe the transition. Maris *et al.* (*5*) have proposed and tried several methods for supercooling H_2 drops. Other groups have studied the behavior of thin H_2 films on various substrates (*6, 7*) or have tried to exploit finite size effects in confined geometries, such as occur in porous media (*8, 9*), but so far without success.

The present research was inspired by the Feynman path integral Monte Carlo (PIMC) simulations of Sindzingre *et al.* (*10*), who found that small pH_2 clusters with only 13 and 18 molecules exhibit a superfluid transition below ~2 K, whereas clusters with 33 molecules did not. They attributed this effect to the 30% decreased density resulting from the large surface-to-volume ratio and the related reduced coordination in the small clusters. To identify the transition in a given cluster, they calculated its effective moment of inertia and angular momentum, both of which are known to vanish in a superfluid at temperatures well below T_c (*1*).

In the present experiments, the recently discovered phenomenon of "molecular superfluidity" (*11*), which refers to the free rotations of single molecules [and small clusters (*12, 13*)] inside superfluid ^{4}He, has been exploited to search for superfluidity inside small OCS-$(oD_2)_n$ and OCS-$(pH_2)_n$ clusters with n = 14 to 17. The central OCS (linear carbonyl sulfide) molecule in these small clusters serves as a spectroscopic probe for measuring the effective moments of inertia. Its symmetry axis also provides an axis of angular momentum quantization without having any inherent angular momentum, as is known from the gas-phase spectrum and also found in liquid ^{4}He droplets (*14*). By coating the large ^{4}He droplets with a thick outer layer of ^{3}He, which has a lower evaporative temperature, it is possible to fix the temperature in the interior of the ^{4}He core at either 0.38 K (without ^{3}He) or 0.15 K (with ^{3}He). The evidence for superfluidity of the pH_2 clusters is derived from changes in the high-resolution infrared (IR) spectra of the OCS-$(pH_2)_n$ (n = 14 to 16) clusters, which occur upon lowering the temperature from 0.38 to 0.15 K. The disappearance of the Q-branch spectral feature, which is associated with vibrational transitions between states with the same rotational quantum numbers (Δj = 0), indicates a vanishing of the angular momentum around the symmetry axis (*15*). This is consistent with a large decrease in the effective moment of inertia, as expected for the transition to a superfluid state. Further confirmation comes from a lack of any effect in OCS-$(oD_2)_n$ clusters, where, as discussed above, the onset of superfluidity is greatly impaired.

The coaxial laser-droplet beam depletion apparatus was identical to that described in (*11, 13*). The lead salt diode laser was tuned to the 0 → 1 vibrational transition of the stretch mode (2060 cm^{-1}) of the OCS chromophore molecule inside helium droplets. The droplets were produced by expanding 99.9999% pure ^{4}He or ^{3}He gas, or a mixture consisting of 4% ^{4}He in ^{3}He, at P_o = 30 bar and T_o = 8.5 K through a 5-μm nozzle. The OCS molecules were first combined with the droplets in a separate scattering chamber at an optimal pressure of 3×10^{-6} mbar, such that on average 0.4 OCS molecules were captured per droplet (*12*). Then, either 99% pure pH_2 or 96% pure oD_2—produced by low-temperature catalytic conversion of liquid H_2 or D_2, respectively—was added in a second liquid nitrogen–cooled scattering chamber at pressures corresponding to the addition of an average number of $\bar{n}$ = 15 molecules. Upon attachment of the H_2 or D_2 molecules, they form small clusters around the OCS molecule that resides near the center of the droplet (*12*). In the mixed ^{4}He/^{3}He droplet, a nearly pure ^{4}He phase surrounds the impurity; in turn, this phase is coated by ^{3}He, which extends to the outside (*11, 16*). The beam of droplets is detected by a quadrupole mass spectrometer. The absorption of photons from the laser beam leads to a large decrease in the detector signal.

To monitor the number of hydrogen molecules added, we first measured the spectra in pure ^{3}He droplets, in which the rotational structure is shrunk into a single peak, simplifying its assignment (*11*). Spectra at relatively high oD_2 and pH_2 pick-up pressures exhibit a series of well-separated peaks shifted toward the red and separated by ~0.3 to 0.5 cm^{-1} (Fig. 1, A and B). These peaks could each be assigned to a particular value of n (*12, 13*). The additional anomalous peaks in the oD_2 spectrum (Fig. 1A, asterisks) were assigned to clusters in which one of the oD_2 molecules is replaced by a pD_2 molecule, which at 4% is the major impurity in the oD_2 supply gas. Also, the shifts of the peaks corresponding to OCS-$(pH_2)_n$ for n = 12 and 13 as well as for n = 15 and 16 are anomalous in that they lie too close together (Fig. 1B). Because the latter anomalies are not seen in pure ^{4}He droplets (Fig. 2C), they may be due to small structural differences. Otherwise, the peak shifts follow a smooth dependence up to n = ~17 for both pH_2 and oD_2 (Fig. 1C). The nearly identical shifts for the two hydrogen isotopes indicate that they have similar structures. The dependence saturates for larger n, indicating the completion of the first shell around the OCS molecule. The line shifts corresponding to the formation of the second and third shells are much smaller because the molecules are farther away from the central chromophore and the corresponding bands are no longer resolved.

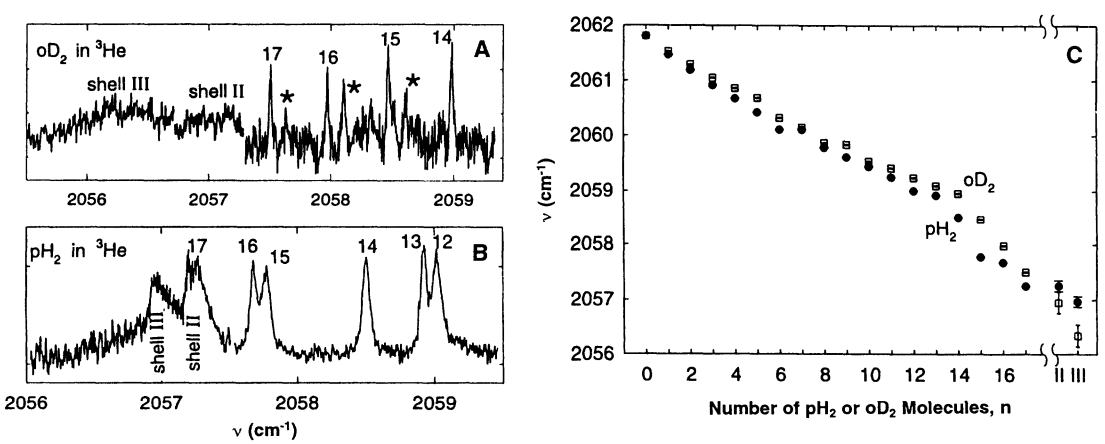

Fig. 1. Spectra of OCS-$(oD_2)_n$ clusters (**A**) and OCS-$(pH_2)_n$ clusters (**B**) inside pure ^{3}He droplets, consisting of about 5000 atoms, in the frequency region where the first shells are completed and the second and third shells are filled. The asterisks denote peaks resulting from the inclusion of pD_2 impurities. (**C**) Measured frequencies of the collapsed spectra of OCS-$(pH_2)_n$ and OCS-$(oD_2)_n$ clusters inside ^{3}He droplets are plotted as a function of n.

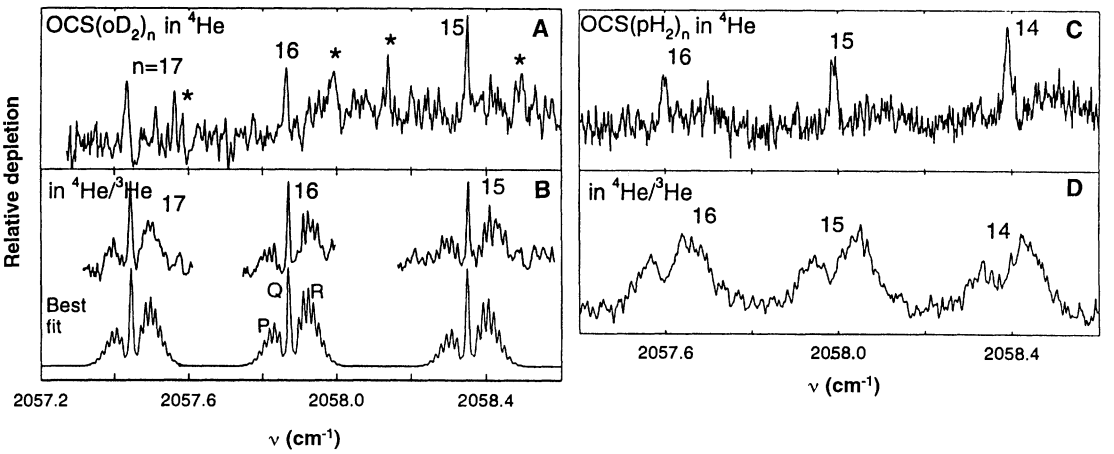

Fig. 2. Comparison of the IR spectra measured for three different OCS-$(oD_2)_n$ and OCS-$(pH_2)_n$ clusters in helium droplets. (**A** and **B**) OCS-$(oD_2)_n$ clusters with n = 15, 16, and 17 in pure ^{4}He droplets with about 8000 atoms (T = 0.38 K) and in mixed ^{4}He/^{3}He droplets with 10,000 ^{3}He atoms and 500 ^{4}He atoms (T = 0.15 K), respectively. (**C** and **D**) OCS-$(pH_2)_n$ clusters with n = 14, 15, and 16 in the same droplet environments. The asterisks in (A) denote peaks resulting from the inclusion of pD_2 impurities. The bottom part of (B) shows best-fit simulations based on a free symmetric top Hamiltonian with spectral resolution of $\delta\nu$ = 0.01 cm^{-1}.

In the oD_2 spectra measured in pure ^{4}He droplets (Fig. 2A), the P- and R-branches—which correspond to transitions to rotational states that differ in their rotational quantum numbers by $\Delta j = -1$ or $\Delta j = +1$, respectively—are largely obscured by noise. However, the sharp Q-branch is clearly seen for each of the clusters. In the colder mixed ^{4}He/^{3}He droplets (Fig. 2B), a distinct Q-branch and the rotational lines of the P- and R-branches are well resolved. In all three pH_2 clusters in Fig. 2C, the Q-branches once more are clearly observed, but surprisingly they disappear in the three much better resolved spectra measured in the mixed ^{4}He/^{3}He droplets (Fig. 2D).

To quantify these results, we simulated the spectra using the Hamiltonian for a freely rotating top that is symmetric about the OCS axis (*17*). It was not possible, however, to properly account for the effect of nuclear spin statistics because the symmetry of the H_2 clusters is not known. With the exception of the very noisy traces for the oD_2 clusters in the pure ^{4}He droplets (0.38 K), the experimental spectra could be well simulated, as exemplified by the best-fit calculations for the oD_2 clusters in ^{4}He/^{3}He mixed droplets (0.15 K) shown in Fig. 2B. The assumption of a symmetric top structure is confirmed by the good agreement of the frequencies and the intensities of the resolved rotational lines with the simulations. The rotational envelope of the pH_2 spectra could also be nicely fitted by assuming the previously established temperatures of T = 0.38 K and 0.15 K for the ^{4}He and ^{4}He/^{3}He droplets, respectively (*11, 12*) (Fig. 3, C and D). From the best fits, the symmetric top moments of inertia I_A and I_B, which correspond to rotations around the OCS molecular axis and perpendicular to it (Table 1), are obtained via the rotational constants A and B using the relations $I_A = \hbar^2/2A$ and $I_B = \hbar^2/2B$. Because a Q-branch could not be detected in the pH_2 spectra at T = 0.15 K, only an upper limit for I_A can be estimated.

The experimental values of I_B for the oD_2 and pH_2 clusters (Table 1) are considerably greater than expected for the free cluster. For a free OCS-$(oD_2)_{17}$ cluster, the total value for I_B is estimated to be ~1030 amu·Å^2 (*14*). Thus, the observed value is larger than expected for the free cluster by a factor of 2.5. For the corresponding free pH_2 cluster, if the structure were identical, a value of ~557 amu·Å^2 would be anticipated because the mass is smaller by a factor of 2. The observed values are greater by a factor of ~3.0. These ratios are in line with the factor of 2.8 increase in I_B for a bare OCS molecule in a ^{4}He droplet (*11, 14*).

Despite the large noise in the pH_2 spectra at T = 0.38 K, values in the range 600 to 1000 amu·Å^2 could be obtained for I_A. These values are significantly higher than the expected value of 360 amu·Å^2. At 0.15 K the value of I_A nearly vanishes, as indicated by the disappearance of the Q-branch (Fig. 2D). Compared to the oD_2 clusters at the same temperatures, I_A is more than an order of magnitude smaller, whereas on the basis of the reduced mass I_A should at most be only about a factor of 2 smaller.

To confirm that I_A changes significantly between 0.38 K and 0.15 K, it is necessary to rule out the possibility that the disappearance of the Q-branch is a consequence of the reduction in the Boltzmann factor due only to the lowering of the ambient temperature. We therefore simulated the pH_2 cluster spectrum at T = 0.38 K using the 0.15 K parameters (Fig. 3E) and the spectrum at 0.15 K using the 0.38 K parameters (Fig. 3F). In both cases, the measured spectra (Fig. 3, A and B) differ considerably from the simulations, especially with respect to the presence of the Q-branch. Thus, the observed effect is not explained by a temperature-induced change in the populations of the rigid symmetric top rotational degrees of freedom, but is due to a large inherent reduction in the effective moment of inertia I_A. Precisely this behavior is expected for a superfluid cluster.

Table 1. Vibrational band origin frequencies ν and best-fit symmetric top moments of inertia I_A and I_B as a function of the number of oD_2 or pH_2 molecules for the spectra in Fig. 2. The temperatures are 0.38 K in the pure ^{4}He droplets and 0.15 K in the mixed ^{4}He/^{3}He droplets. Numbers in parentheses are the estimated mean square deviations in the last significant digits. Asterisks denote insufficient resolution for a reliable determination of the rotational constants.

n	Droplet	ν (cm^{-1})	I_A (amu·Å^2)	I_B (amu·Å^2)
		oD_2		
15	^{4}He	2058.35(1)	*	*
	^{4}He/^{3}He	2058.35(1)	510 (170)	2380 (40)
16	^{4}He	2057.86(1)	*	*
	^{4}He/^{3}He	2057.87(1)	730 (190)	2550 (40)
17	^{4}He	2057.44(1)	*	*
	^{4}He/^{3}He	2057.44(1)	1050 (260)	2810 (140)
		pH_2		
14	^{4}He	2058.39(1)	670 (350)	1530 (140)
	^{4}He/^{3}He	2058.39(1)	<56	1770 (150)
15	^{4}He	2057.99(1)	990 (700)	1530 (280)
	^{4}He/^{3}He	2057.99(1)	<56	1870 (210)
16	^{4}He	2057.60(1)	600 (450)	1670 (70)
	^{4}He/^{3}He	2057.60(2)	<56	1870 (210)

Other possible explanations, such as changes in the ^{4}He superfluid fraction, can also be excluded because at these low temperatures, the ^{4}He normal fluid fraction in large droplets is expected to be similar to the bulk value, which is only $\sim 10^{-6}$. The small concentration of ^{3}He, which is estimated to be less than 2% in the vicinity of the cluster (*16*), is also not expected to affect rotational motion at either temperature (*18*). The only structural change that could explain the decrease in I_A involves a realignment of all the pH_2 molecules away from the tightest binding sites near the waist to positions at the pole caps, thereby forming a linear configuration along the axis of rotation. This seems very improbable in view of the much weaker van der Waals binding at the cap sites (*19*) and is not consistent with the regular behavior of the line shifts in Fig. 1.

The observed striking differences in the behavior for oD_2 and pH_2 therefore are most likely due to the different permutation symmetries resulting from the different nuclear spin states (see Eq. 1). If the oD_2 or pH_2 shells are cursive, then the point group symmetry with respect to the OCS axis will be important. Such a rigid cluster may be viewed as consisting of several coaxial rings of D_2 (H_2) molecules arranged along the OCS axis. The overall symmetry of several concentric rigid rings, each with different numbers of molecules (with $n < 6$), will be much lower than for a single ring with six ^{4}He atoms (C_{6v}), which just fits around the waist, as was recently postulated to exist for OCS molecules in pure superfluid ^{4}He droplets (*14*). As a result of the lower symmetry and large number of attached D_2 (H_2) molecules, the rotations should be energetically allowed even at 0.15 K, as indicated by the oD_2 cluster spectra. However, if the system is sufficiently cursive so that exchange permutations between the cluster molecules are possible, then the particle spins become important in determining the dynamical behavior in much the same way as discussed by Feynman (*20*). Feynman argued that the superfluid is characterized by closed loops of helium atoms resulting from Bose permutation exchange symmetry. This concept is at the basis of the Feynman PIMC method for simulating superfluidity. Thus, because of the corresponding high symmetry of such liquid shells about the OCS axis, the corresponding low-energy rotations would be energetically forbidden, which is equivalent to a decrease in the effective moment of inertia, as is observed. On the basis of these arguments, we conclude that our results indicate the onset of superfluidity in the pH_2 clusters, which is not found in the oD_2 clusters.

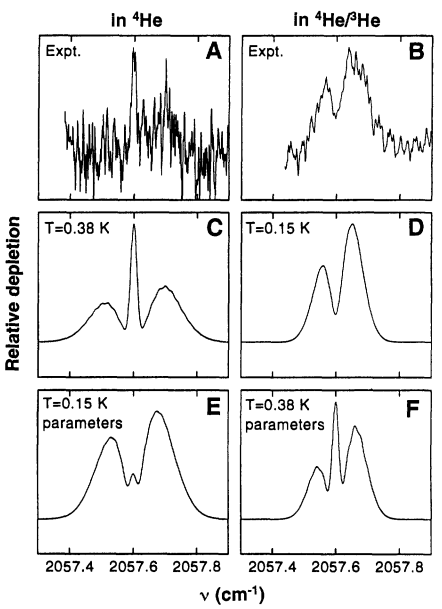

Fig. 3. Two typical measured spectra for OCS-$(pH_2)_{16}$ clusters (**A** and **B**) are compared with best-fit simulations (**C** and **D**) for temperatures of 0.15 and 0.38 K, respectively. In (**E**) the spectrum at 0.38 K is simulated using the best-fit rotational constants of the data at 0.15 K. The very low intensity of the Q-branch in the simulation indicates that these rotational constants cannot explain the observed spectrum. In (**F**) the spectrum at T = 0.15 K is also not reproduced by a simulation using the parameters obtained at 0.38 K. Thus, the difference in the experimental spectra cannot be explained by the changes in Boltzmann factors at the two temperatures. A spectral resolution of 0.02 cm^{-1} was assumed in the fits (C to F) taken from the averaged width of the Q-branches in the experimental spectra of Fig. 2C.

These conclusions are consistent with what is now known about small pure cold H_2 and D_2 clusters. Theoretical simulations predict pure oD_2 clusters to solidify at temperatures below 4 K (*21*), whereas small $(pH_2)_{13}$ clusters remain fluid (*21–25*). The main difference between these simulations as well as those of Sindzingre *et al.* (*10*) for pure pH_2 clusters and our experiments is the presence of the OCS chromophore at the center of the cluster and the embedding of the entire cluster inside superfluid helium. The effect of an impurity has been studied in the PIMC simulations of lithium-containing $(pH_2)_n$ clusters for n = 13, 55, and 180 carried out by Klein and co-workers (*26*), even though they did not test for superfluidity. Their simulations at ~2 K revealed that the small $Li(pH_2)_n$ clusters are completely melted and have a self-diffusion coefficient similar to that of bulk liquid pH_2 (*27*). The effect of the outer helium environment has recently been simulated using the PIMC method for small H_2 clusters (n = 6 and 13) inside larger ^{4}He clusters with up to 40 atoms at 0.5 K (*28*). These calculations indicate a clear separation of the two species with a slightly compressed central H_2 cluster and a decrease in the H_2 superfluid fraction from ~0.45 (n = 6) to ~0.10 (n = 13). The strong interaction with the OCS chromophore and the presence of the ^{4}He atoms on the outside are thus expected to reduce the transition temperature from the calculated value of 2 K for the pure clusters in the direction of the order of magnitude smaller value found here.

References and Notes

1. P. Nozières and D. Pines, *The Theory of Quantum Liquids, Vol. II: Superfluid Bose Liquids* (Addison-Wesley, Reading, MA, 1990).
2. F. Dalfovo, S. Giorgini, L. P. Pitaevskii, S. Stringari, *Rev. Mod. Phys.* **71**, 463 (1999).
3. V. L. Ginzburg and A. A. Sobyanin, *JETP Lett.* **15**, 242 (1972).
4. F. London, *Nature* **141**, 643 (1938).
5. H. J. Maris, G. M. Seidel, T. E. Huber, *J. Low Temp. Phys.* **51**, 471 (1983).
6. F. C. Lui, Y. M. Lui, O. E. Vilches, *Phys. Rev. B* **51**, 2848 (1995).
7. H. Wiechert, *Physica B* **169**, 144 (1991).
8. D. F. Brewer, J. C. N. Rajendra, A. L. Thompson, *J. Low Temp. Phys.* **101**, 317 (1995).
9. M. Schindler, A. Dertinger, Y. Kondo, F. Pobell, *Phys. Rev. B* **53**, 11451 (1996).
10. P. Sindzingre, D. M. Ceperley, M. L. Klein, *Phys. Rev. Lett.* **67**, 1871 (1991).
11. S. Grebenev, J. P. Toennies, A. F. Vilesov, *Science* **279**, 2083 (1998).
12. J. P. Toennies and A. F. Vilesov, *Annu. Rev. Phys. Chem.* **49**, 1 (1998).
13. M. Hartmann, R. E. Miller, J. P. Toennies, A. F. Vilesov, *Science* **272**, 1631 (1996).
14. S. Grebenev *et al.*, *J. Chem. Phys.* **112**, 4485 (2000).
15. Because of conservation of angular momentum, a Q-branch corresponding to $\Delta j = 0$ can only be observed if the spin of 1 of the photon can be transferred to the molecule. This is not possible for a linear molecule with a transition dipole along the axis of symmetry, but becomes allowed if the projection of the angular momentum on the axis is nonzero, as in the case of a symmetric top with angular momentum along the axis of symmetry, $K > 0$.
16. M. Pi, R. Mayol, M. Barranco, *Phys. Rev. Lett.* **82**, 3093 (1999).
17. G. Herzberg, *Infrared and Raman Spectra of Polyatomic Molecules* (Van Nostrand, Princeton, NJ, 1945), pp. 400–446.
18. J. Harms, M. Hartmann, B. Sartakov, J. P. Toennies, A. F. Vilesov, *J. Chem. Phys.* **110**, 5124 (1999).
19. K. Higgins, personal communication.
20. R. P. Feynman, *Phys. Rev.* **91**, 1301 (1953); *Phys. Rev.* **94**, 262 (1954).
21. D. Scharf, G. J. Martyna, M. L. Klein, *Chem. Phys. Lett.* **197**, 231 (1992).
22. E. Cheng, M. A. McMahon, K. B. Whaley, *J. Chem. Phys.* **104**, 2669 (1996).
23. M. A. McMahon and K. B. Whaley, *Chem. Phys.* **182**, 119 (1994).
24. D. Scharf, M. L. Klein, G. J. Martyna, *J. Chem. Phys.* **97**, 3590 (1992); K. Kinugawa, P. B. Moore, M. L. Klein, *J. Chem. Phys.* **106**, 1154 (1997).
25. C. Chakravarty, *Mol. Phys.* **84**, 845 (1995); *Phys. Rev. Lett.* **75**, 1727 (1995).
26. K. Kinugawa, P. B. Moore, M. L. Klein, *J. Chem. Phys.* **106**, 1154 (1997).
27. We note, however, that the van der Waals well depth for the orientation-averaged interaction of Li and H_2, $\varepsilon \approx 15$ K [see figure 3A in C. Cheng and K. B. Whaley, *J. Chem. Phys.* **104**, 3155 (1996)], is much weaker than the orientation-averaged well depth of $\bar{\varepsilon} \approx 70$ K recently calculated by Higgins for OCS-H_2 (*19*). Moreover, the Li atoms are at the surface and not in the interior.
28. M. C. Gordillo, *Phys. Rev. B* **60**, 6790 (1999).

29. We thank D. Ceperley, Y. Kagan, and B. Whaley for valuable discussions and comments, N. Pörtner for assistance in preparing the figures, and K. Higgins for sending us his potential calculations.

26 April 2000; accepted 10 July 2000